TD-006-004
01/27/06

# Proton Driver Front End
# Focusing Solenoid Quench Protection Studies.
# Part II: Test Solenoid Quench Protection

I. Terechkine

In [1], where the method of this analysis was suggested and tested by making the first iteration step, we used the approximation of a constant current and came to the conclusion that if the power supply is made off immediately following the quench, the current ought to decay due to the rise of the coil resistance. Fig. 1 presents graphs of the corresponding current shapes. Several analytical representation of this effect can be suggested to simplify later work; the next one has been chosen at this stage:

$$I(t, I_0) = \frac{2 \cdot I_0}{1 + \exp\left[\left(\frac{t \cdot I_0}{46}\right)^{2.8}\right]}$$

Fig. 1 compares this representation (right graph) with the results obtained in [1] numerically.

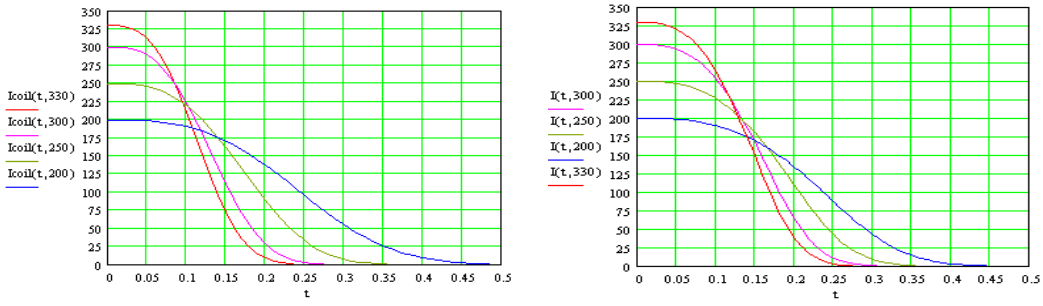


Fig. 1: Coil current: the first iteration

The coil resistance obtained during the first iteration (constant current approach) is clearly higher than what can be in reality, when current decays with time; so, "real" current profile will be more "stretched" in time. To find the "real" current profile, we need to recalculate coil resistance dynamics using the new current shape.

## I. The Second Iteration Run

We will accept the "first iteration" output parameterized current shape to start the second iteration in the attempt to converge on the final current shape. The "convergence" means that after several iterations, the current shape accepted at the beginning of the process will be close to the current shape obtained in the end.

The expression for the delay of quench propagation between the layers that we used in Part I of this study (Fig. 20) must be modified now taking into the account that the current changes with time explicitly:

$$Delay(n,I0,t) := if\left[Ic(t,I0) > 190, if\left[n < 17 - 6\cdot10^{-4}\cdot(330 - Ic(t,I0))^2, 2.3\cdot10^{-4}\cdot n + 2.2\cdot10^{-6}\cdot(330 - Ic(t,I0))^{1.5}, 2.3\cdot10^{-4}\cdot\left[17 - 6\cdot10^{-4}\cdot(330 - Ic(t,I0))^2\right] + 2.2\cdot10^{-6}\cdot(330 - Ic(t,I0))^{1.5}\right], 0.005\right]$$

Dependence of this delay on the layer number is only because the magnetic field linearly changes towards the outer radius of the solenoid.

If the current changes in time, delay of the quench front propagation in any position "m, n" inside the coil will also explicitly depend on time. This is illustrated by the plot shown in Fig. 2. For the first layer, as the quench front propagates from turn to turn,

current becomes smaller and corresponding delay time becomes larger until it reaches the saturation value when the critical temperature becomes close to its ultimate value: 9.2 K. For layers inside the coil, magnetic field is lower, resulting in longer delay.

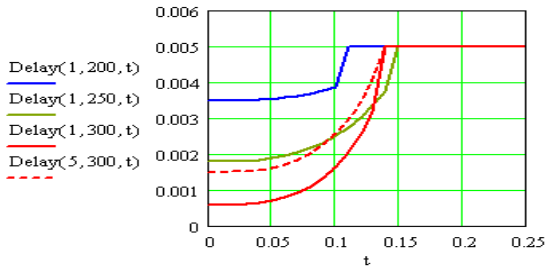


Fig. 2: Time delay versus time

There is one computational problem though: now if we need to find when the front of the quench comes to the position "m,n" in the coil, for each turn on the quench front, the explicit time must be used that takes the front to come to this particular point. So, we come to a recurrent operation, which means that the delay for quench front to reach "m,n" position is a function of delays on a way to this position. It was not so difficult to right this recurrent expression, but it took too much time to the solver to solve it for even 25 points (we need 55 x 20). So, we are forced to find a way to resolve the issue. One of the ways to go is to write a simple step-by-step instruction for MathCad, get a series of data within the range of interest for each of parameters, and then to parameterize results. Corresponding subroutines are shown below:

1. For the longitudinal propagation along the first layer:

$$i := 0..55$$

$$Dax_0 := 0$$

$$Dax_1 := Dax_0 + Delay(1, I0, Dax_0)$$

$$Dax_{i+1} := Dax_i + Delay(1, I0, Dax_i)$$

2. For the radial propagation from the first layer to the layer "j" in the plain containing the turn "i":

$$j := 0, 1..20$$

$$D_{i,0} := Dax_i$$

$$D_{i,j+1} := D_{i,j} + Delay(j, I0, D_{i,j})$$

The results obtained using this approach were compared with the results obtained earlier for the constant current in the graphs in Fig. 3, where the constant current data are in the left column, and the data with the current changing in time are on the right.

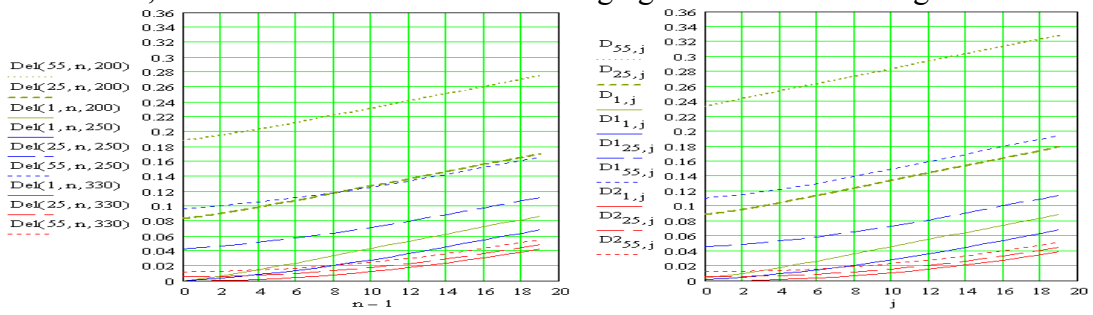


Fig. 3: Quench front propagation delay time

To proceed with the analysis we need to find a simple expression for the delay of the quench front propagation to the internal point of the coil "m, n", similar to what was used during the first iteration. The next expression was used this time (see also Fig. 4):

$$Del1(m,n,I) = Del(m,n,I)\cdot(1.6 - 2\cdot10^{-3}\cdot I)\cdot(1+1\cdot10^{-3}\cdot m)$$

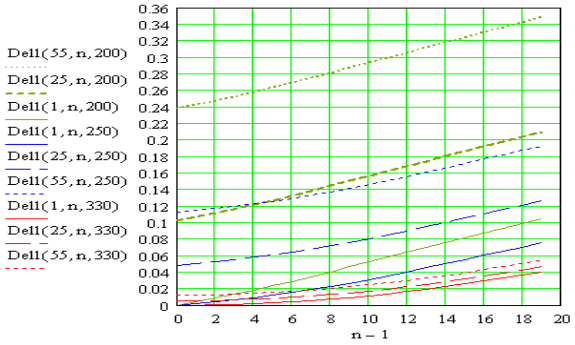


Fig. 4: Quench front propagation delay time for the second iteration.

Comparing the graphs in Fig. 3, not much of change in propagation delay can be notices at any current in the radial direction for the cross-section that is perpendicular to the axis and pass through the center of the solenoid (m = 1; solid curves). Obviously this happens because quench can quickly propagate radially to the point where delay almost does not depend on the current. For the section that passes though the axial position corresponding to m = 25 (dashed curves), only at low current we notice some increase of delay, that almost does not depend on the layer number. The reason is similar to what was found earlier: during axial propagation, current does not decay much to develop significant change in the delay time and during the radial propagation, the delay time saturates because the effective current drops linearly with the layer number. For the section that passes though the axial position corresponding to m = 55 (dotted curves), one can see some increase in the delay time for high currents, noticeable increase for the intermediate currents and relatively high delay for the low currents. The underlying reason of this behavior is that at high current quench front reaches the position m = 55 when current did not change much yet; then during radial propagation, the delay time quickly reaches saturation. At the intermediate current and low current, the quench front reaches this position at the moment when the current is already significantly lower than in the very beginning of the process.

As it was done in chapter IV of the "first iteration" note [1], it is possible now to find IIT and temperature of each turn as a function of time. For IIT, it is necessary to use more general expression than was used earlier:

$$IIT1(m,n,I0,t) := \text{if}\left(t - Del1(m,n,I0) > 0, \int_{Del1(m,n,I0)}^{t} Ic(x,I0)^2\,dx, 0\right)$$

A series of graphs in Fig. 5 should be compared with the corresponding graph in Fig. 24 of [1]. The initial parts of the curves (up to the moment t = 0.1 s) are quite close, but, due to current decay, IIT-s quickly saturate to their maximal value. It is necessary to state that these graphs do not exactly reflect the reality because of the initial assumption of how the current changes with time. If the real current is decaying with time faster, coil temperature will be a bit less and so will be less the coil resistance. This in turn will result

in longer current decay. So, there is a clear negative feedback in the calculation process because the temperature of the turns depends on the resistance and current, which, in turn, depends on the temperature.

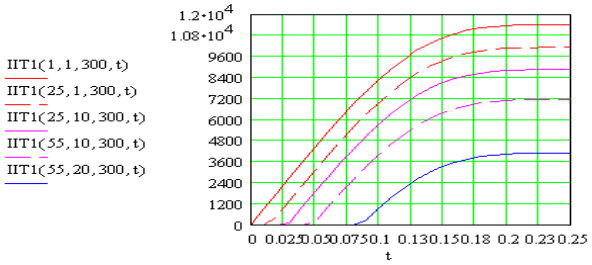


Fig. 5: The second iteration IIT(t) for turns in the coil.

Temperature of the turns can be found by applying the relationship between the IIT-s and the temperature shown in Fig. 22 of [1]. Graphs of turn temperature for maximal current are shown in Fig. 6. The temperature in the coil does not exceed 90 K.

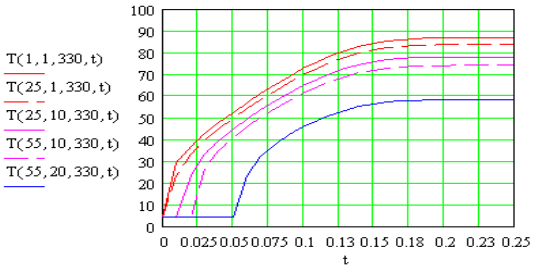


Fig. 6: Temperature of the turns versus time at maximal current

Based on the known temperature of the turns, their resistance can be found using the expression in the chapter IV of the Part I [1]:

$$R(m,n,I,t) := \text{if}\left(t > \text{Del}(m,n,I), \frac{2\cdot\pi\cdot\text{rad}(n)}{\text{Atot}}\cdot\text{rhocomp}(T(m,n,I,t)), 0\right)$$

The only difference is that now we have different temperature profile T(m,n,I,t). One can expect saturation of the resistance of every turn to its maximal value because the temperature saturation (Fig. 6). Corresponding curves are shown in Fig. 7 and must be compared with Fig. 25 of [1]. The initial parts of the curves look quite similar, but for t>0.15 s, the curves start saturating.

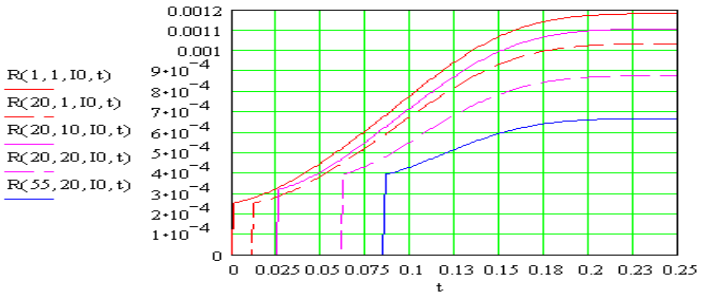


Fig. 7: Resistance of coil's turns during quench

Resistance of every layer can found by taking a sum of turn resistances in that layer. Corresponding graphs for different currents are presented in Fig. 8.

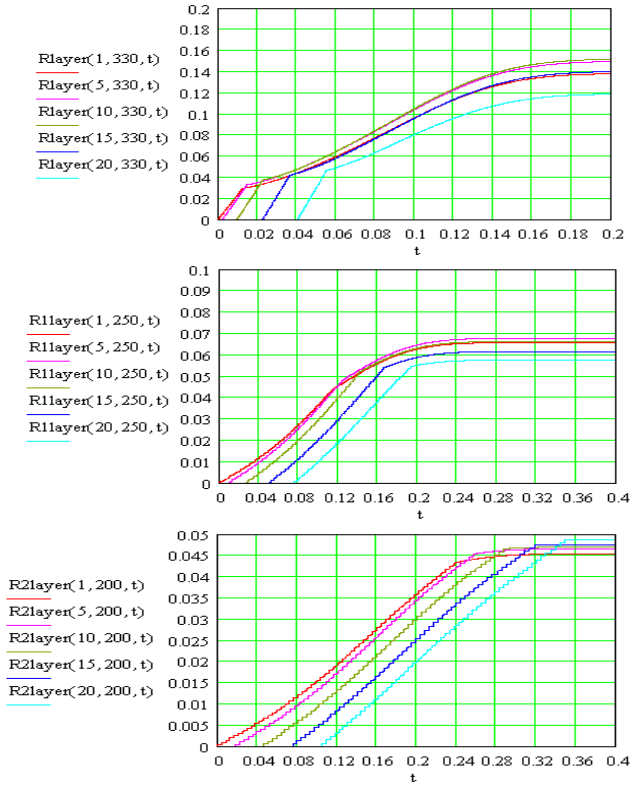


Fig. 8: Layer resistance at different currents

**At 330 A**, we see three distinctive parts in the graph: initial sharp rise of the resistance, gradual smooth resistance rise, and saturation. The initial part is explained by quench propagation along the layer. Here quick transition from superconducting to the normal state occurs that results in the sharp resistance rise. The next part is due to the gradual temperature rise as a result of the accumulated IIT-s. Saturation part obviously starts after current decays completely. **At 250 A**, quench propagation is slower, and by the time it propagates through the layers, current is already significantly lower then its maximal value, and hence less time is left for the gradual temperature rise of the whole layer and the saturation part is closer to the sharp rise part. **At 200 A**, the first, sharp rise part immediately followed by the saturation part. It can happen at this current that not all the turns turn normal.

The total coil resistance is a sum of layer resistances. It is found at every moment in time for different levels of the initial current ***I0*** (Fig. 9).

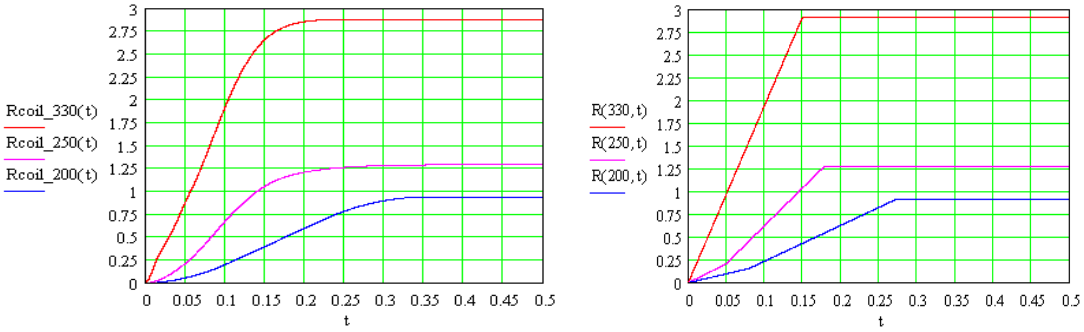


Fig. 9: Coil resistance at different starting currents

To save computation time, an appropriate parameterization was made for the layer resistance and for the coil resistance. Corresponding piece-wise expression for the coil resistance is shown below, and the graphs are shown on the right side of Fig. 9.

$$Rm(I) := 0.94 + 9.36\cdot10^{-5}\cdot(I - 186.5)^2$$

$$ti(I) := 0.08 - \frac{0.08}{130}\cdot(I - 200)$$

$$k2(I) := 2.5 + \frac{15}{130}\cdot(I - 200) + 4\cdot10^{-4}\cdot(I - 260)^2$$

$$te(I) := 0.15 + 5.6\cdot10^{-8}\cdot(330 - I)^{3.0}$$

$$R(I,t) := \begin{cases} \left\langle \frac{k2(I)}{2}\cdot t \right\rangle & \text{if } t \le ti(I) \\ \left[ \frac{k2(I)}{2}\cdot ti(I) + k2(I)\cdot(t - ti(I)) \right] & \text{if } ti(I) < t \le te(I) \\ \left[ \frac{k2(I)}{2}\cdot ti(I) + k2(I)\cdot(te(I) - ti(I)) \right] & \text{otherwise} \end{cases}$$

Based on the new coil resistance, we can find the "second iteration" current shape. It is shown on the left side of Fig. 10 compared with the input current shape on the right.

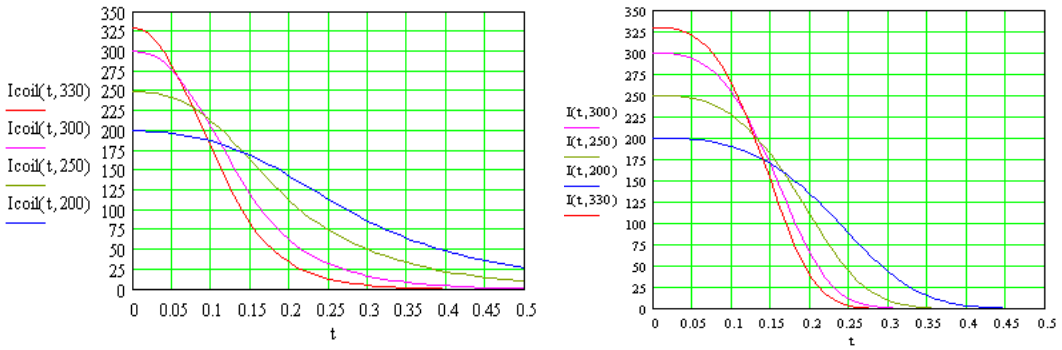


Fig. 10: The second iteration current shape

Comparing graphs in Fig 10, we notice some difference. Now the current is decaying at slower rate. As it was expected, this happened because during the first iteration constant current was used as a starting point. This resulted in faster temperature rise, higher resistance, and shorter resultant current pulse. During the second iteration, we came to a lighter heating, lower resistance and longer current pulse. So, we do have a negative feedback as an intrinsic feature of this problem.

It appears convenient to choose an analytical representation of the current shape in Fig. 10 so that it could be easy to use it during the third (and hopefully the last) iteration. A simple parametric expression can be suggested:

$$I3(t, I0) = \frac{I0}{1 + \left[ \frac{t \cdot I0}{0.3 * A(I0)} \right]^{2.5}}$$

with A(I0) = 200-9/13*(*I0*-200)
Corresponding curves are shown in Fig. 11 and should be compared the curves in Fig. 10.

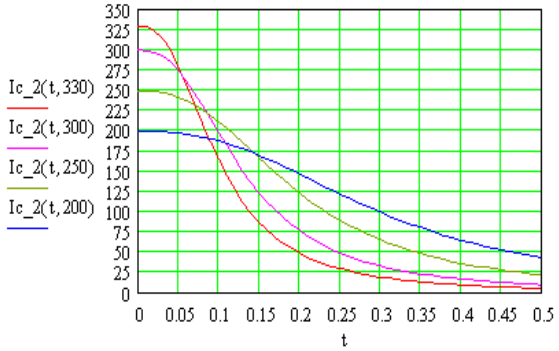


Fig. 11: The second iteration output current shape (parameterized)

The parameterization works quite well, and we can use this expression for the current profile as an input to the third iteration run.

## II. The Third Iteration Run

The expression for the delay of quench propagation between the layers that we used during the second iteration can be used without any modifications here. The quench front propagation delay becomes longer because the second iteration current profile is sharper in the beginning. This can be verified by comparing graphs in Fig. 12 with the similar one obtained during the second iteration (Fig. 2).

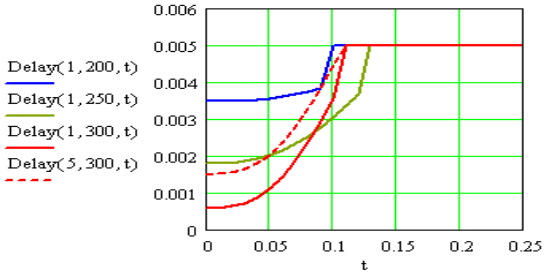


Fig. 12: Time delay versus time

The quench front propagation delay time to the turn “m,n” can be found similar to what was done during the second iteration. Corresponding graph is shown in Fig. 13.

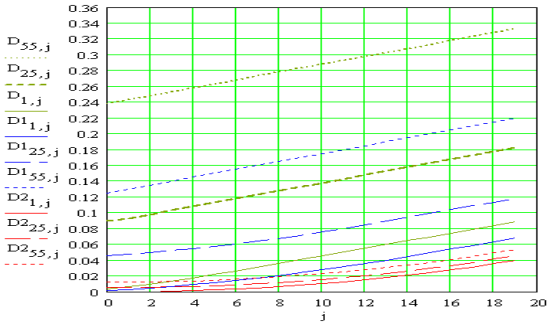


Fig. 13: Quench front propagation delay time

The next expression was used for parameterization of this set of data (compare with the similar expression accompanying Fig. 4):

$$Del1(m,n,I) := Del(m,n,I)\cdot\left[1 - 8.4\cdot10^{-4}\cdot\left(\frac{m}{25}\right)^{2.7}\cdot(I-330) - 1.15\cdot10^{-6}\cdot\left(\frac{m}{25}\right)^{4.5}\cdot(I-330)^2\right]$$

With the known current shape and delay of the quench front propagation, we can find IIT-s of each turn of the coil. Corresponding graph for *I0* = 300 A is shown in Fig. 14 and must be compared with the Fig. 5.

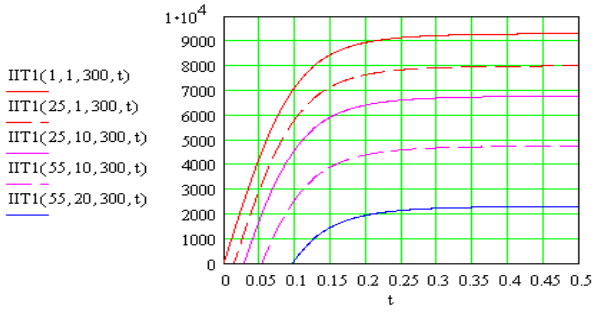


Fig. 14: The second iteration IIT(t) for turns in the coil.

The temperature of the turns can be found, as before, using $T_{peak}$ function, which is a function of material properties. Corresponding graphs for the current of 330 A are shown in Fig. 15. The maximal temperature in the coil reaches ~70 K in about 150 ms.

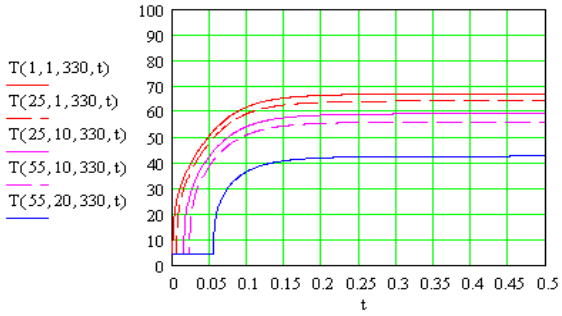


Fig. 15: Temperature of the turns versus time at maximal current

Based on the temperature dynamics, we can evaluate resistance of each turn at every moment in time. Corresponding curves are shown in Fig. 16 and must be compared with Fig. 7 in this note and with Fig. 25 in [1].

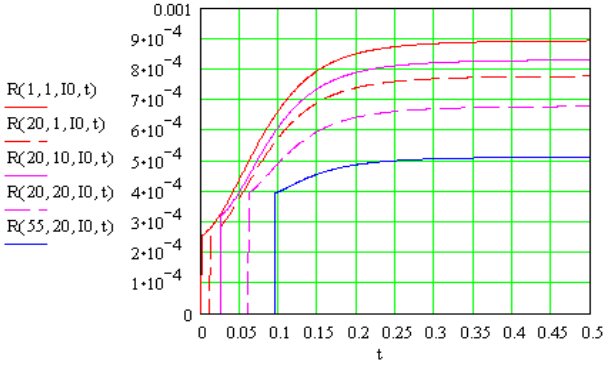


Fig. 16: Resistance of coil's turns during quench

As before, resistance of layers is found by taking a sum of turn resistances in the corresponding layer. Corresponding graphs for different currents are presented in Fig. 17 and should be compared with Fig. 8.

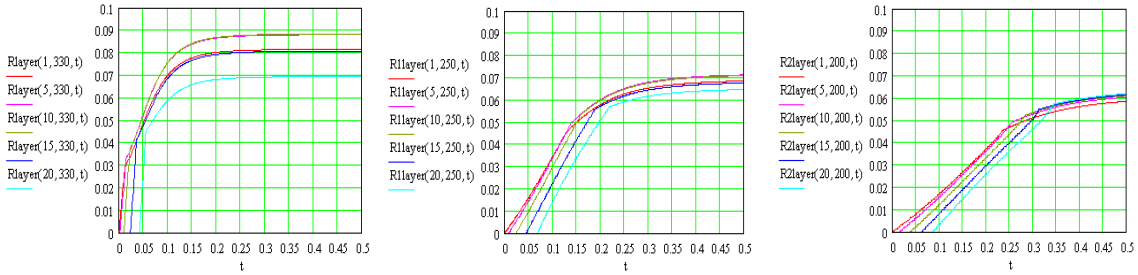


Fig. 17: Layer resistance at different currents

As earlier, the coil resistance can be found by summing the resistances of the layers at every moment and for different values of the initial current *I0*. Corresponding graphs are presented in Fig. 18 and can be compared with Fig. 9.

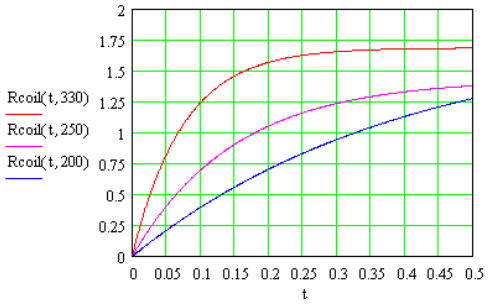


Fig. 18: Coil resistance at different starting currents

Knowing behavior of the coil resistance in time, it is straightforward to find the resultant third iteration current shape. Fig. 19 below compares it with the current shape used as input for the third iteration (Fig. 11).

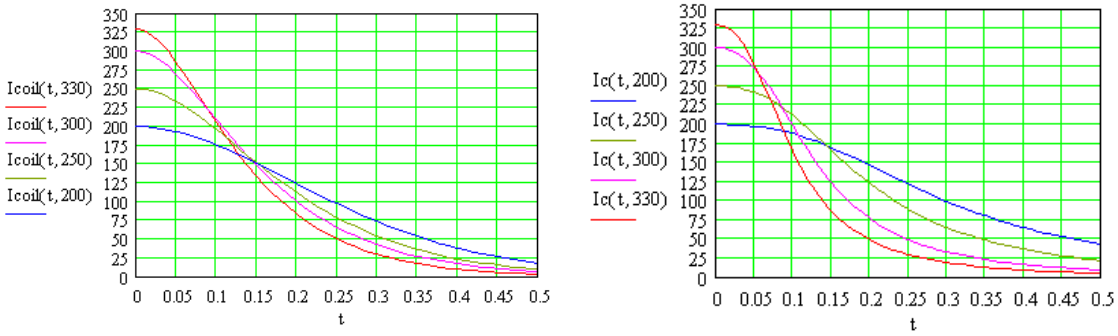


a) output current shape b) input current shape

Fig. 19: Third iteration output and input current shape

Comparing the two graphs in Fig 19, we can see some difference, although time frame of the current decay did not change much. At maximal current, the decay goes a bit slower, and for lower current – a bit faster. This is an indication that the iterations have almost converged, but the analytical representation of the current shape we've chosen is not a perfect one.

It was quite possible to make the fourth iteration to further converge on the current shape, but with multiple parameterizations made to get this result, we should expect a high level of a "computational noise" with amplitude that can exceed expected accuracy.

To get exact results, one needs to perform honest calculation using an appropriate code or develop one. So, at the moment, we will end with an analytical representation of the third iteration output current shape:

$$A(I0) := 47 - 2.3\cdot 10^{-6}\cdot(I0 - 200)^3$$

$$Ic1(t, I0) := \frac{I0}{1 + \left(\frac{t\cdot I0}{A(I0)}\right)^{2.2}}$$

Corresponding graph is shown in Fig. 20. This representation should be compared with the output current shape in Fig. 19.

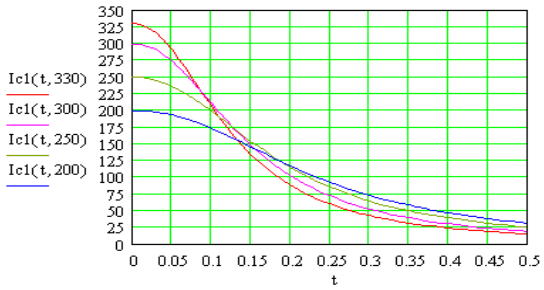


Fig. 20. Output current shape for the third iteration (analytical representation).

An uncertainty of this analytical representation can be evaluated by calculating the coil voltage. Resistive and inductive components of the voltage are shown in Fig. 21.

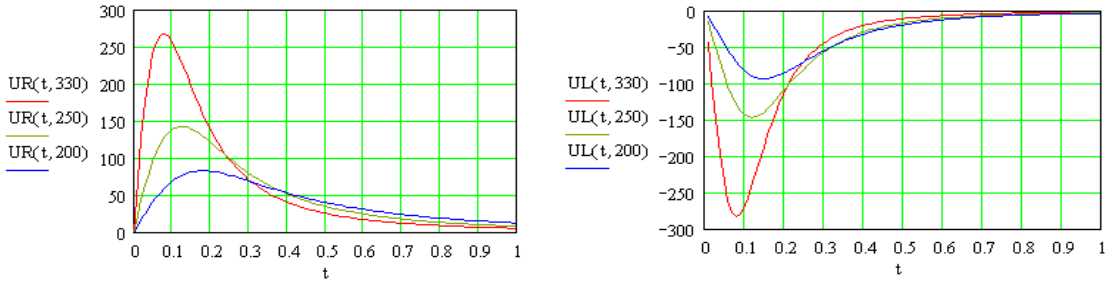


Fig. 21: Resistive and inductive voltage in the coil.

Theoretically the sum of these components must be exactly zero. Fig. 22 shows the sum, which is about 10% of the partial voltages and oscillates around zero level. This indicates that the analytical representation of the current shape is not quite perfect, but for our purpose this precision looks OK.

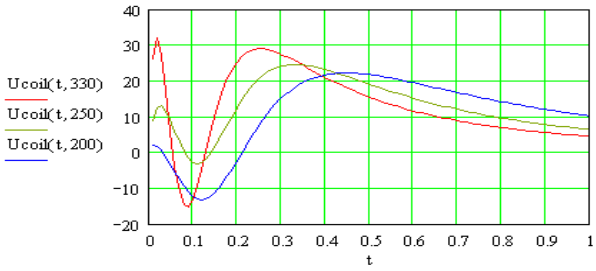


Fig. 22: Total voltage across the coil's leads.

# III. Quench Protection

Knowing how resistance and current change with time, it is possible to make analysis of issues related to quench protection. First thing to understand is whether the coil can be protected by switching off the power supply and **shortening its leads through a diode**, which usually works well for small-scale solenoids.

We will start with the integrated (through the total coil) energy deposition:

$$Q(t, I0) := \int_0^t UR(x, I0) \cdot Ic1(x, I0)\, dx$$

Corresponding graphs are shown in Fig. 23. Even for 200 A current the energy stored in the magnetic field of the coil is almost fully transferred into heat in about 0.5 seconds. For higher currents this process goes even faster (within 0.3 seconds for I = 330 A). This result shows that coil protection issues must be properly addressed to ensure safe operation. On the other hand, the total energy deposition in the coil is quite modest, so we can expect that coil of this size can be self-protected.

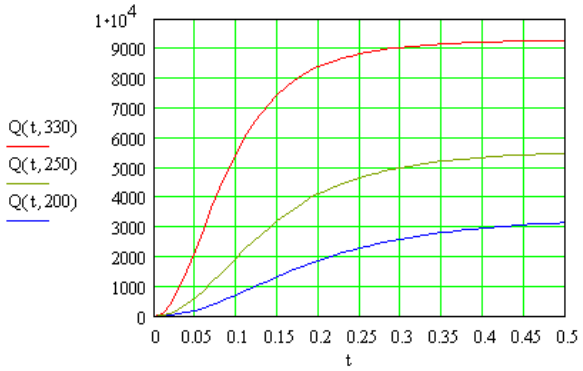


Fig. 23. Heat deposition in the coil.

Detection of quench can be based on measurement of the voltage drop across the whole coil or its part. During this detection stage, the current supply is still on and the current time derivative at the moment of the quench onset is small. So, it is possible to evaluate the coil voltage rise based only on the coil resistance dynamics. The change of the resistive voltage with time after quench is shown in Fig. 21 above.

Immediately after the quench, the voltage rise rate is ~ 7.5 V/ms for 330 A initial current, ~ 2.5 V/ms for the 250 A, and ~ 1.0 V/ms for the 200 A current. Taking into the account the quench detection time of ~1 ms, it seems safe to accept the detection threshold of ~1 V. After coil voltage reaches 1 V, the power supply must be made off

Additional energy deposited in the coil before the protection system switches the power supply off will be defined by the existing current and the dynamics of the resistance change: this gives power deposition rate of less than ~ 10 J/ms at I0 = 330 A, which is small compared with the total stored energy in the coil of ~ 10 kJ.

Another thing to worry about is maximal voltage in the coil relatively to the ground. To find this quantity, we need to know not only resistances of all layers, but also their mutual inductances. The next set of expressions was used to find layer inductance and the mutual inductance of any two layers of the coil located at radii R1 and R2:

$$L1(R) := \frac{4\cdot 10^{-7}\cdot \pi^2 \cdot wl^2 \cdot R^2}{1 + 0.9\cdot R}$$

$$M(R1,R2) := \frac{4\cdot \pi^2 \cdot 10^{-7}\cdot wl^2 \cdot (if(R2<R1,R2,R1))^2}{1}\cdot\left[1 - \frac{if(R2<R1,R1,R2)}{1}\cdot\left(1 - \frac{if(R2<R1,R2,R1)}{8\cdot if(R2<R1,R1,R2)}\right)\right]$$

The total inductance of the coil can be found by summing through all the layers:

$$L := \sum_{i=0}^{N1-1}\sum_{j=0}^{N1-1} if(i=j, L1(R_i), M(R_i,R_j))$$

Taking this sum for the geometry of the coil, we find **L = 0.16 H**, which agrees well with the value obtained by direct computation of the total coil inductance.

Reactance of any specific layer is a sum of its inductance and all the mutual inductances with all other layers. Knowing the reactance, it is possible to find the inductive voltage drop for any specific layer. To get the resistive voltage, we will use the layer resistances found earlier (Fig. 17). By taking a sum through the layer from 1 to n of the inductive and the resistive voltage, we can obtain information about the voltage to ground in the coil. Because the outer layer of the coil is shorted to the first layer, this voltage should have its maximum somewhere inside the coil. Fig. 24 shows distribution of this voltage inside the coil at different moments: 1ms, 10 ms, 50 ms, 100 ms, 150 ms, and 200 ms.

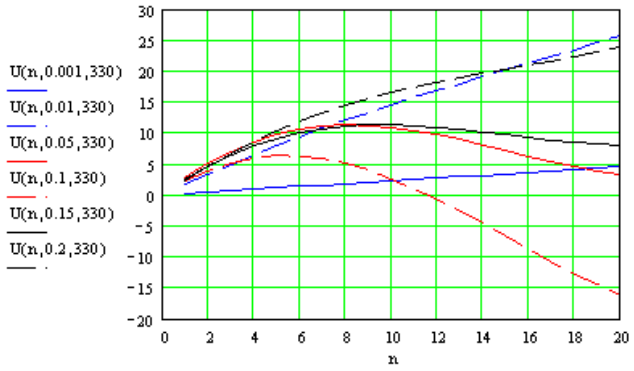


Fig. 24: Layer-to-ground voltage distribution inside the coil.

Early in time, we see only the resistive component of the voltage because the current have not started to drop yet in our analytical representation of the current shape. In reality it should start though to make the total voltage at n = 20 equal to zero. Starting ~ 50 ms, we see that resistive voltage is compensated by the inductive one for every turn. It can be under-compensated or over-compensated for each layer to result in a particular layer to ground voltage at this point. Again the voltage at n = 20 is not equal to zero here, which is an uncertainty of this model. At later times, the current decay rate becomes lower, and the layer resistances grow with time resulting in the residual resistive voltage. At any moment in time we see that the layer to ground voltage is below ~ 30 V, which is on the level of ~ 10% of the maximal resistive or inductive voltage. Results at n = 20 correspond to the voltage of the total coil, and in a good agreement with what was shown in Fig. 22 for I0 = 330 A.

Maximal voltage between layers can be found as a doubled derivative of the graph in Fig. 24. By analyzing this graph, we can see that this voltage does not exceed ~ 5 V.

The next questions worth to ask is whether an **external dump resistance** can help dissipating power outside a cryostat? Positive answer means a potential for saving LHe, associated power, and time to heat and cool down solenoids.

In the case of the external resistive load, current shape will be mainly defined by this load and in lesser degree, by the dynamics of the coil resistance. So, we will accept a model when the coil heating is found in the approximation of a constant current (we have learned earlier that this is about true for at least the first 50 ms) and find the current decay rate having in mind the constant external resistance and changing coil resistance. The expression for the analytical approximation of the coil resistance was given in Part I of this study [1]. Corresponding graph is reproduced in Fig. 25. The initial part of this graph is quite similar to that in Fig. 9.

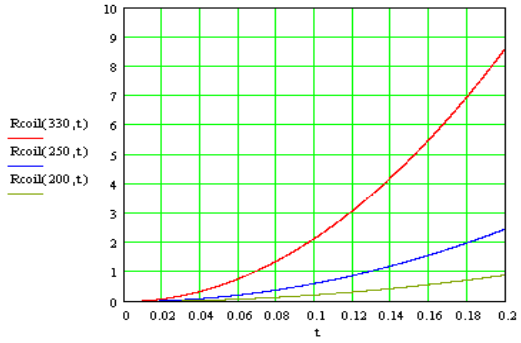


Fig. 25: Coil resistance dynamics at different quench current levels

The total circuit resistance is now $R(I0,t) = R_{coil}(I0,t) + R_{dump}$ and the shape of the decaying current is now described by

$$Icoil(t, I0) := I0 \cdot \exp\left[ - \int_0^t \frac{R(I0, x)}{Lcoil} dx \right]$$

At different values of the damp resistor we will have different sets of the current decay curves with the initial current as a parameter. The set of the curves for $R_{dump}$ = 1 Ohm is shown in Fig. 26.

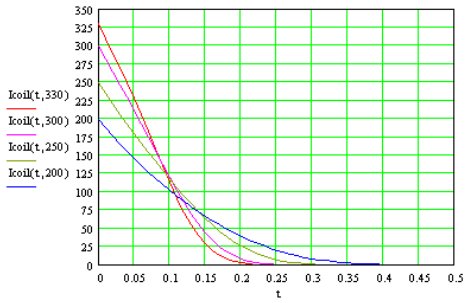


Fig. 26: Current decay curves at $R_{dump}$ = 1 Ohm

Now, as we know the current decay details, it is straightforward to find total energy dissipated by the dump resistance. For example, for the 330 A initial current

$$Qdump := \int_0^{0.5} Icoil(t, 330)^2 \cdot Rdump\, dt$$

Comparing this energy with the total energy stored in the coil before the quench, we can find the effectiveness of a dumping resistor. For the 330 A current, corresponding graph is shown in Fig. 27:

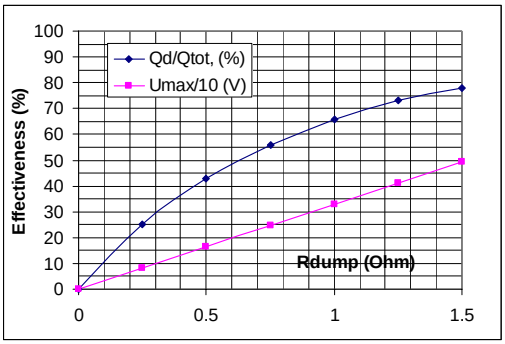


Fig. 27: Effectiveness of a dump resistance as a function of the value of the resistance

With the dump resistance, maximal voltage in the coil changes accordingly. So, the resistance can not be too large to have an acceptable total voltage. At the coil leads, the voltage can not exceed $I \cdot R_{dump}$, but inside the coil one can expect higher voltage. Fig. 27 shows how the voltage changes with the resistance. Based on this graph, we can tell that the resistance of 1 Ohm can help removing 65% of the total energy stored in the coil outside and the voltage will not exceed ~ 400 V, which is still acceptable from the point of view of coil insulation system.

The next thing to consider is whether the coil needs **quench heaters.** Using heaters helps to create additional normal zones within the coil thus distributing the total energy within the coil more evenly. As a result, maximal temperature after the quench will be lower.

## IV. Quench Heater

Because, as it has been shown, quench propagation in the solenoid is quite fast, it is important to understand a typical time that takes the coil to quench after the heater is activated and a required energy deposition in the heater.

Let's first answer the latest question. The heater is usually made of stainless steel (or other low conductivity alloy) foil that is arranged in a certain pattern to reach needed resistance. To start approaching the heater design, we will assume certain parameters of a pulser to power the heaters. This assumption is based on the available in IB-1 power supply used to activate heaters of the LHC magnets. It uses pulsed discharge of a capacitor bank with **C = 2400 μF** , charged with the voltage up to **V = 400 V,** through the heaters. The allowed current is $\mathbf{I_m}$ **= 200 A**. To obtain maximal power during the shortest time, the resistance of the heaters must be as low as possible, but it can not be lower than 2 Ohm if full allowable voltage is used.

We will further assume that two identical side heaters are working in parallel – this gives the resistance of each heater of ~4 Ohm at 4 K. Specific resistance of stainless steel

SS-304 at 4K is ~ $5 \cdot 10^{-7}$ Ohm·m. So for the 50 μm thick, 1-mm-wide foil, the total length of the foil strip becomes 0.5 m.

The total volume of the heater material is then ~ ρ*L*w*t ≈ 25 $mm^3$. The energy required to bring the temperature of this mass to the level of about 300 K can be found if we know enthalpy of this material at different temperatures. A satisfactory approximation of the heat capacity of stainless steel 304 ($J/m^3K$) and its enthalpy ($J/m^3$) as a function of temperature is shown in Fig 28:

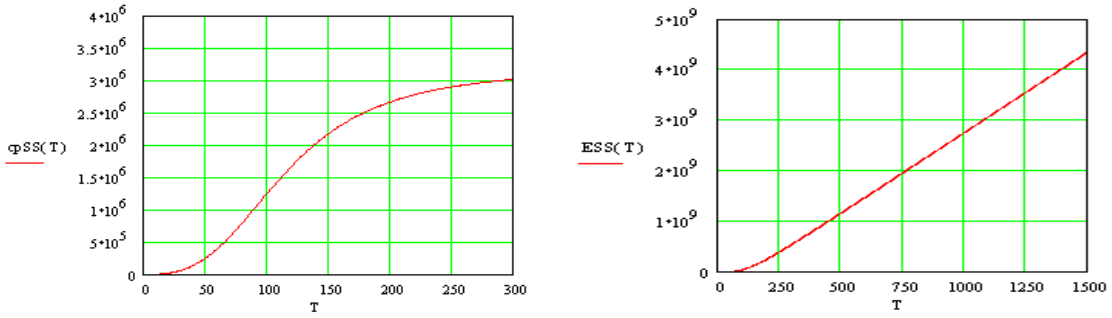


Fig. 28: Specific heat and enthalpy of stainless steel 304.

Energy deposition in one pulse is $W = 1/2CU^2 \approx 200$ J. At 400 V, this corresponds to ~100 J for each heater or ~$4*10^9$ $J/m^3$. The expected heater temperature can be found from Fig. 28: it can reach ~1500 K. Because the heater insulation can not withstand this temperature, clearly we need to limit the level of the charging voltage. If to limit the temperature of the heater to about 500 K ( ~ 200 C), which Kapton insulation can reliably withstand, we come to maximal charging voltage of ~200 V. Fig. 29 shows the heater temperature dependence of the charging voltage.

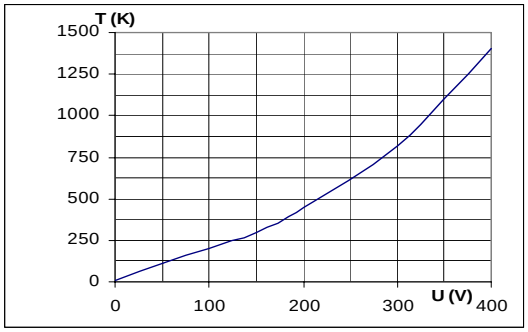


Fig. 29: Heater temperature as a function of the charging voltage (C = 2400 mkF)

So, we came to the point where we can tell what maximal energy deposition in the heater we can afford and on what time scale this deposition can be made:

W = 25 J per heater

τ = RC = 5 ms

The next question is how quickly can this heat be transferred to the nearest layer of a superconductor and bring its temperature above the critical level of 9.2 K. The method used to answer the question was similar of that used to study quench propagation across layers of the coil. The heat transfer problem was modeled using time-step modeling of foil heating, heat transfer though the layer of Kapton insulation separating the heater from the coil winding, and the temperature increase of the NbTi strand. Specific heat of NbTi was taken as it was defined during quench modeling. Thermal conductivity of Kapton

depends on temperature quite weakly, so average value of ~0.04 W/m-K was accepted through all the range of the temperature change. Thickness of the Kapton insulation of 0.2 mm was accepted for this run.

Power density in the heater reaches 100 W/mm$^2$ at maximal current of ~100 A per one heater (at 400 V), but decays quickly as current decays (Fig. 30).

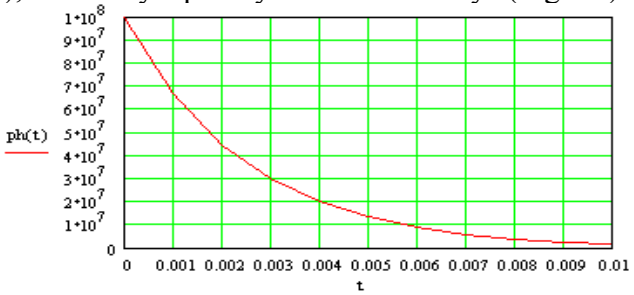


Fig. 30: Power deposition rate for the heater.

Graphs showing the temperature rise in the heater and in the NbTi strand are shown in Fig. 31. Note the x10 scale for the strand temperature. On the same graph, critical temperature of NbTi is shown as a line parallel to the time axis.

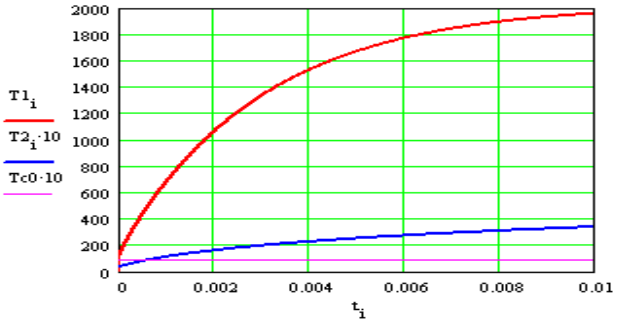


Fig. 31: Heater (red) and strand (blue) temperature change in time

One can immediately notice very slow rate of temperature rise in the strand. Nevertheless, the strand quenches well before the current decays that tells that the heater should work to help the coil to quench. Also we see that the maximal temperature of the heater foil reaches almost 2000 K, that agrees with the high heater temperature at 400 V charging voltage estimated earlier.

Changing the heater current, it is possible to vary power density in the heater. As a result, quench delay time will change. Corresponding graph is shown in Fig. 32.

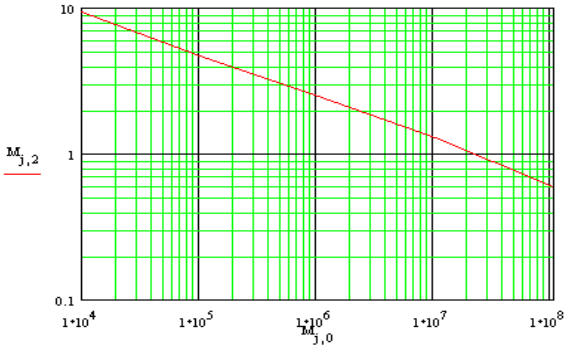


Fig. 32: Time delay (ms) as a function of the heater power density (W/m$^2$)

Here the vertical axis gives quench delay in milliseconds at the range of power densities (in W/m$^3$) along the horizontal axis. It is possible to notice very weak dependence of the quench start delay on the power density: One order of magnitude in the delay time is reached after power density was changes by four orders of magnitude (or current changed by two orders of magnitude).

As a result of this weak dependence, the pulser parameters can be chosen so that the heater temperature is kept at minimal level that insures safe work of the device. The graph in Fig. 33 shows heater temperature (K) as a function of the heater maximal power density (W/m$^2$), that can be compared with Fig. 29.

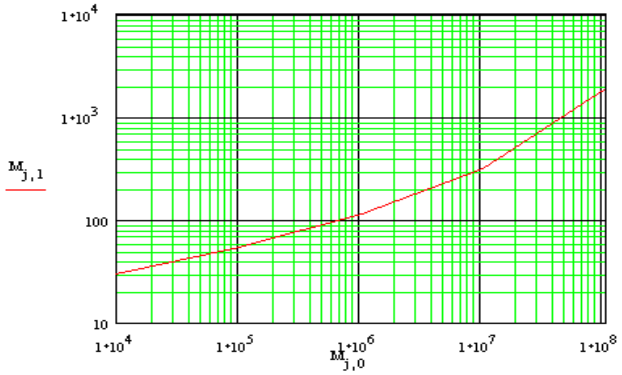


Fig. 33: Heater temperature (K) as a function of the heater power density (W/m$^2$)

Comparing Fig. 32 and Fig. 33 (or Fig. 29), one can tell that it would be quite safe to work in the region of p = 1*10$^7$ W/m$^2$ (I = 35 A per one heater, U = 140 V) to ensure delay time of less than 1.5 ms with the maximal heater temperature of less that 400 K, which is OK for the Kapton insulation.

Changing thickness of the Kapton insulation results in corresponding change in the coil quench delay time. As it is shown in Fig. 34 for p = 10$^8$ W/m$^2$, changing the thickness twice results in approximately twice as fast heat transfer. So, making insulation thickness equal to 100 μm (instead of 200 μm that was accepted in this note) will make the quench delay at 10$^7$ W/m$^2$ of less than 1 ms.

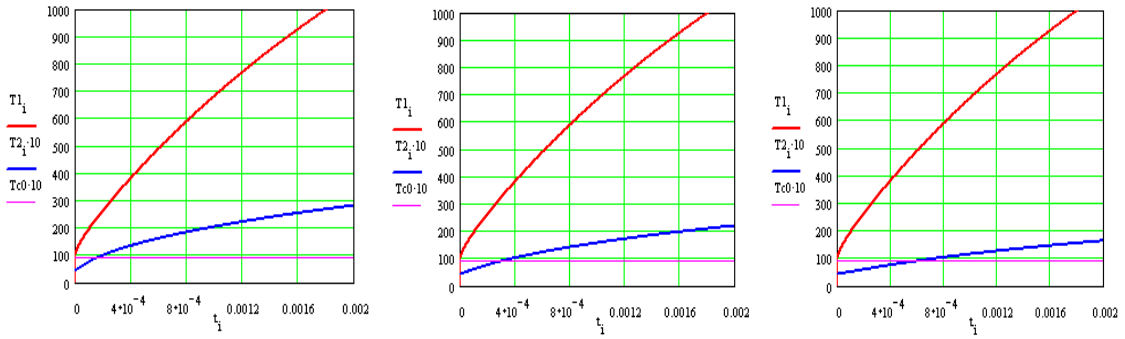


a) $t_{ins}$ = 50 μm b) $t_{ins}$ = 100 μm c) $t_{ins}$ = 200 μm

Fig. 34: Time delay as a function of Kapton insulation thickness (p = 10$^8$ W/m$^2$)

Applying the same method to the heater at room temperature, one gets much longer delays (of the order of ~ 10 ms) even for thin insulation. This happens because of a significant difference in the material properties at 4.5 K and 300 K.

# V. Summary

1. Quench front propagation issues have been analyzed for the superconducting solenoid of a Proton Driver Front End focusing channel.
2. It was shown that propagation of quench in the radial and axial direction is mainly due to thermal conductivity of the insulation between the layers and turns in the coil.
3. Solenoid coil is self-protected to the quench in the sense that the maximal temperature in the coil does not become too high before current decays after the power supply is made off by a quench detection system.
4. It is possible to use a dump resistance with R ~ 1 Ohm to extract a part of the total stored energy outside the solenoid cryostat.
5. It is possible to consider using heaters for "assisted quenching" to lower maximal coil temperature.
6. The chosen method of quench analysis, although allowed reaching some convergence in the current shape, did not guarantee high accuracy. The indication of this is the absence of full convergence in the total coil voltage. Significant simulation noise is probably an intrinsic feature of the chosen method. More reliable data can be obtained if a special program is used that allow for step-by-step modeling of the thermal processes in the coil.